Deformation of light xenon isotopes

S. Raman
Oak Ridge National Laboratory, Oak Ridge, Tennessee 37831

J. A. Sheikh*
Joint Institute of Heavy-Ion Research, Oak Ridge, Tennessee 37831

K. H. Bhatt
Department of Physics and Astronomy, University of Mississippi, University, Mississippi 38677

(Received 6 April 1995)

Recently measured $B(E2;0_1^+ \rightarrow 2_1^+)$ values for the light xenon ($Z=54$) isotopes show a marked increase in deformation as the neutron numbers approach the midshell value of $N=66$. At first sight, this behavior is anomalous because the 2_1^+ level energies are nearly the same for these isotopes. Moreover, this increase is not readily explained by several nuclear models that assign single shells to valence protons and neutrons. In particular, the single-shell asymptotic Nilsson model with current parameters seriously underpredicts the $B(E2;0_1^+ \rightarrow 2_1^+)$ values for $^{118}Xe_{64}$, $^{120}Xe_{66}$, and $^{122}Xe_{68}$. On the other hand, several modern multishell models correctly predict these values. We examine the latter results more closely to find ways in which the single-shell asymptotic Nilsson model can be revised to correctly reproduce the measurements. We also show that the $B(E2;0_1^+ \rightarrow 2_1^+)$ values for lighter ($N<66$) barium isotopes, when they are measured, will test the predictive power of existing systematics and modeling of quadrupole deformations in nuclei.

PACS number(s): 21.60.Cs, 21.60.Ev, 21.60.Fw, 27.60.+j

I. INTRODUCTION

The deformation of the nuclear ground state is a fundamental property that can be deduced in even-even nuclei from the $B(E2)$ value for the first 2^+ state (2_1^+). In 1987, we published a compilation of such $B(E2;0_1^+ \rightarrow 2_1^+)$ values for ~ 280 even-even nuclei [1]. With this compilation as a starting point, we tested various systematic, empirical, and theoretical relationships that have been proposed in connection with these values [2–8]. We also generated some new systematics of our own. We showed that a variety of tools now exist to test whether a newly measured $B(E2;0_1^+ \rightarrow 2_1^+)$ value is consistent with our current understanding of ground-state (quadrupole) deformations and to make reliable predictions for those nuclei lacking experimental values.

These theoretical tools can be divided into three broad categories—global, regional, and universal. (i) According to the global systematics, a knowledge of the energy E of the 2_1^+ state is all that is required to make a prediction for the corresponding $B(E2;0_1^+ \rightarrow 2_1^+)$ value. (ii) If the magic numbers are taken into account, a variety of regional schematic models exist that can make predictions with expressions containing at most three adjustable constants. (iii) State-of-the-art universal calculations now exist that have already made (or are capable of making) predictions, based on first principles, for several thousand nuclei between the proton and neutron drip lines. All three types of predictions pertain to all nuclei or to large blocks of them, and thus are absolute in the sense that *ad hoc* renormalizations to improve agreement with the experimental data for a particular element (or a small group of elements) are impermissible.

The $B(E2;0_1^+ \rightarrow 2_1^+)$ values that we recommended in Refs. [1] and [3] were based solely on measured values reported in the literature or communicated to us directly and were not influenced by these systematics and calculations. We chose this policy partly because we felt that if measurements that disagreed (strongly) with systematics were reported (and confirmed), new physics was likely to emerge in attempting to interpret such results.

An early and serious disagreement with systematics occurred in the case of ^{172}W. A preliminary $B(E2;0_1^+ \rightarrow 2_1^+)$ value [9] was reported for this nucleus which was $\sim 50\%$ higher than those for the neighboring ^{170}W and ^{174}W. We questioned this result [10] on the basis of both global and regional systematics. A reexamination of the ^{172}W data [11] led to a value $\sim 20\%$ lower than that originally published. This lower value is reasonably consistent (within the stated uncertainties) with systematics. We have shown elsewhere [7] that the newly measured $B(E2;0_1^+ \rightarrow 2_1^+)$ values for $^{90-96}Sr$, $^{122-126}Ba$, and ^{152}Nd are consistent with global systematics.

The experimental $B(E2;0_1^+ \rightarrow 2_1^+)$ values for the light xenon ($Z=54$) isotopes, especially those for $^{118-124}Xe$, posed special problems while arriving at the values recommended in Refs. [1] and [3]. Of the nine known values for these isotopes, six were from secondary sources (abstracts, conference proceedings, private communication, etc.). Eight of these nine values were deduced indirectly from recoil-distance lifetime measurements, and only one (for the stable ^{124}Xe) was from the more direct Coulomb-excitation data. For ^{122}Xe, there was only a single reported value. Those for

*Visitor from the Tata Institute for Fundamental Research, Colaba, Bombay-400 005, India.

^{120}Xe and ^{124}Xe were badly discrepant. To resolve these discrepancies, we started a dialog with the responsible experimentalists (at Notre Dame and at Köln). This exchange was initially fruitless in that the discrepancy was left unresolved in Refs. [1] and [3]. However, both groups promised to undertake additional lifetime measurements. Their new $B(E2;0_1^+\rightarrow 2_1^+)$ values and those from other sources have now become available. These measurements are inherently difficult, and despite some scatter in the values a reliable picture of the overall behavior of the $B(E2;0_1^+\rightarrow 2_1^+)$ values for the xenon isotopes has begun to emerge as discussed in Sec. II.

Most of the known xenon isotopes are in the $50\leq(Z,N)\leq 82$ ("tin") region. If the behavior of the rare-earth nuclei (whose neutrons are in the next higher shell) is any guide, a small and gradual increase in the xenon $B(E2;0_1^+\rightarrow 2_1^+)$ values is expected as the neutron number is decreased from $N=82$ to the midshell value of $N=66$, then a flattening at midshell, and finally a small and gradual decrease below $N=66$. Instead, the values for the three lightest isotopes, $^{118}Xe_{64}$, $^{120}Xe_{66}$, and $^{122}Xe_{68}$, appear to constitute a small peak. In Secs. III A and III B, we show that existing global and regional models cannot explain this behavior satisfactorily in an *a priori* fashion. In particular, the single-shell asymptotic Nilsson model (SSANM), as currently formulated, fails in the "tin" region. A closer scrutiny of the $B(E2;0_1^+\rightarrow 2_1^+)$ values of the xenon isotopes is, therefore, warranted, and that is the main topic of this paper. In Sec. III C we show that the predictions of universal models are qualitatively different from those of global and regional models. More importantly, several universal models correctly reproduce the absolute $B(E2;0_1^+\rightarrow 2_1^+)$ values and their overall trend for the xenon isotopes. With this hindsight, we reexamine the regional models in Sec. IV. Algebraic models such as the interacting boson approximation (IBA) and fermion dynamic symmetry model (FDSM) are also capable *a posteriori* of reproducing the observed behavior. The deficiencies of the SSANM can be corrected by choosing a different normalization constant for the "tin" region and by considering the influence of Nilsson orbits intruding from the lower shell into the current shell. We justify these modifications in Sec. IV B 3. The $B(E2;0_1^+\rightarrow 2_1^+)$ trend of the light barium ($Z=56$) isotopes, discussed in Sec. V, would be a stringent test of the universal model predictions in the "tin" region. Unfortunately such data are currently unavailable. Our conclusions are given in Sec. VI.

II. $B(E2;0_1^+\rightarrow 2_1^+)$ DATA FOR LIGHT XENON ISOTOPES

Figure 1(a) shows the $B(E2;0_1^+\rightarrow 2_1^+)$ values for the xenon isotopes recommended in the 1987 compilation [1]. For $A\geq 126$, we continue to use these values—except that a preliminary value for $^{138}Xe_{84}$, obtained earlier [12], has been withdrawn [13]. We now wish to examine the data for the lighter ($A<126$) isotopes. All known measurements [14–25], reported before and after the publication of Ref. [1], are summarized in Table I and Fig. 1(b). There are 17 reported values now compared to only 9 in Ref. [1]. All are from lifetime measurements except for one direct Coulomb excitation measurement.

As shown in Table I, the $B(E2;0_1^+\rightarrow 2_1^+)$ values for $^{118}Xe_{64}$ from three separate measurements are consistent with each other. This consistency is especially important because this is the only nucleus below midshell (that is, $N<66$) other than $^{114}Sn_{64}$ for which such measurements have been reported. The $B(E2;0_1^+\rightarrow 2_1^+)$ values for $^{120}Xe_{66}$, on the other hand, cluster around either 0.9 or 1.7 e^2 b^2. Because the experimentalists were cognizant of this discrepancy and, therefore, exercised particular care, we deem the three most recent measurements—which are consistent among themselves and yield a weighted average value of 1.69 ± 0.09 e^2 b^2—as being reliable. The reported value for $^{122}Xe_{68}$ (see Table I) differ by nearly a factor of 2. Petkov *et al.* [24] have made a convincing argument that the high value of 2.00 ± 0.20 e^2 b^2, reported by Droste *et al.* [22], is probably in error because these authors failed to correct the data for the deorientation effect. (Insufficient knowledge of the feeding history is another common difficulty with recoil-distance lifetime measurements.) The remaining three values for $^{122}Xe_{68}$ are reasonably consistent with each other, and we choose the latest value, which also carries the smallest uncertainty. Finally, a preliminary value for $^{124}Xe_{70}$ [19], which disagreed with previous Coulomb-excitation data [25], has been superseded [20] by a revised value (see Table I) that nearly agrees. The newly adopted $B(E2;0_1^+\rightarrow 2_1^+)$ values from Table I, together with the earlier adopted values (except for $^{138}Xe_{84}$) from Ref. [1] for the remaining isotopes, are shown in Fig. 1(c). It is *this* overall trend (and the absolute values) that nuclear models are challenged to reproduce correctly.

III. UNDERSTANDING $B(E2;0_1^+\rightarrow 2_1^+)$ TRENDS

In previous works [2–8], one of our goals was to obtain a general understanding of the $B(E2;0_1^+\rightarrow 2_1^+)$ systematics not only in an empirical fashion but also with simple schematic models [single-particle SU(3), single j, IBA, FDSM, pseudo-SU(3) model (PSM), etc.]. If we now select several representative models and examine whether they can explain the observed $B(E2;0_1^+\rightarrow 2_1^+)$ trends in the xenon isotopes, we find that all of them correctly predict the values for $A\geq 124$ isotopes (near the $N=82$ closed shell), but *underpredict* to varying degrees those for $^{118}Xe_{64}$, $^{120}Xe_{66}$, and $^{122}Xe_{68}$.

A. Global systematics

In Refs. [2] and [3], we showed that the $B(E2;0_1^+\rightarrow 2_1^+)$ values (in units of e^2 b^2) can be obtained from a simple relation

$$B(E2;0_1^+\rightarrow 2_1^+)\approx 3.3E^{-1}Z^{-2}A^{-0.69}, \quad (1)$$

where the energy E of the 2_1^+ state is in keV. For well-deformed nuclei, this relationship arises mainly because a larger $B(E2;0_1^+\rightarrow 2_1^+)$ value implies a larger intrinsic deformation; a larger moment of inertia; and, hence, a lower energy for the 2_1^+ state. These energies are known for ~ 460 nuclei and their predicted $B(E2;0_1^+\rightarrow 2_1^+)$ values (together with their uncertainties) are listed in Ref. [3]. In Fig. 1(d) we compare these predictions for the xenon isotopes with mea-

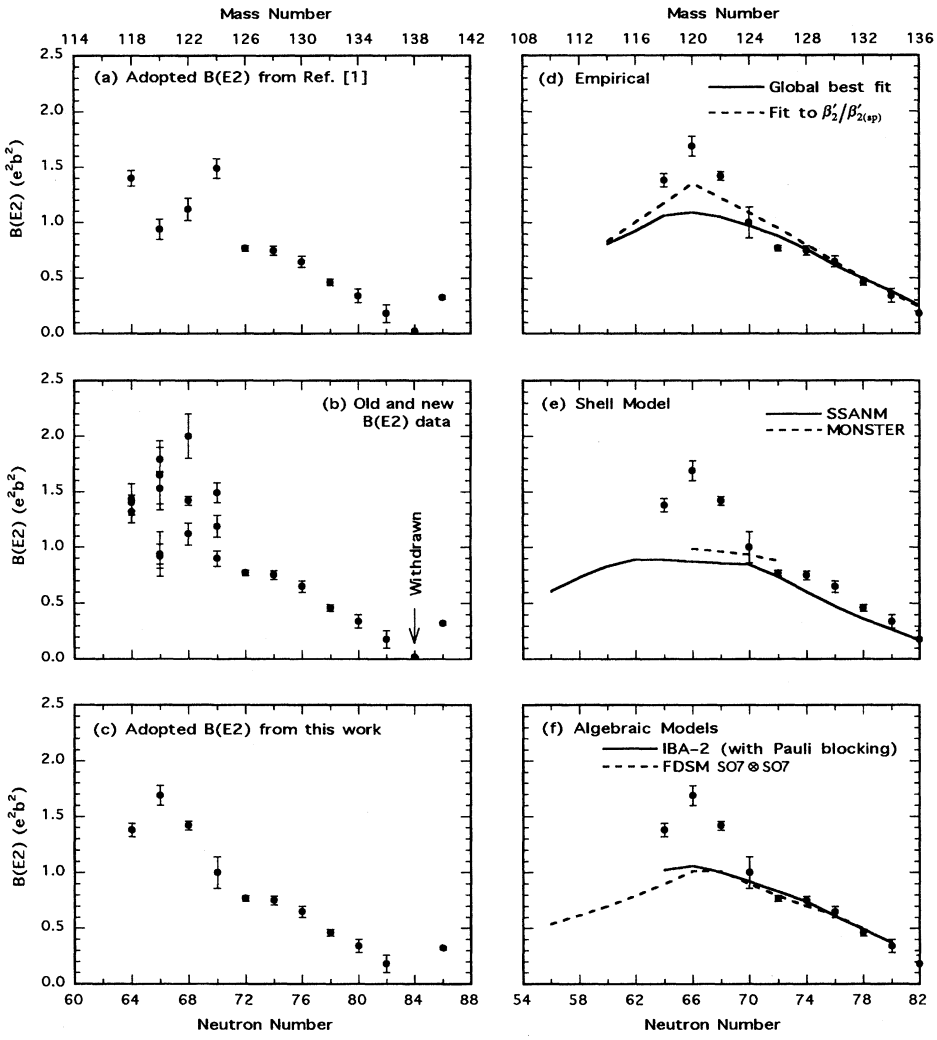

FIG. 1. Comparison between measured (data points with error bars) and calculated (solid and dashed curves) values for the reduced transition probability $B(E2;0_1^+\rightarrow 2_1^+)$ from the ground state to the first excited 2^+ states of even-even xenon isotopes. Measured values shown in (c)–(f) are those adopted in Table I. The different empirical and regional models are discussed in Secs. III A and III B.

surements. The 2_1^+ level energies are nearly the same for the light xenon isotopes (see Table I); therefore, their predicted $B(E2;0_1^+\rightarrow 2_1^+)$ values do not vary greatly. The global systematics clearly underpredict the measured values for $^{118}Xe_{64}$, $^{120}Xe_{66}$, and $^{122}Xe_{68}$.

B. Regional systematics

In Ref. [2], we considered five different regions defined by the magic numbers $Z,N=28$, 50, 82, 126, and 184. We then developed the regional systematics either empirically or through recourse to schematic nuclear models.

1. Empirical $\beta_2'/\beta_{2(sp)}'$ systematics

The parameter β_2' was defined (without the prime) in Ref. [1] as

$$\beta_2'=(4\pi/3ZR_0^2)[B(E2;0_1^+\rightarrow 2_1^+)/e^2]^{1/2}, \tag{2}$$

where $R_0=1.2A^{1/3}$ fm. The single-particle $\beta_{2(sp)}'$ value is given by

$$\beta_{2(sp)}'=1.59/Z. \tag{3}$$

We fitted the $\beta_2'/\beta_{2(sp)}'$ data in each region by an expression of the form

$$\beta_2'/\beta_{2(sp)}'=C+D[1-e^{-\alpha N_p N_n}], \tag{4}$$

where C, D, and α are constants for that region (see Table A of Ref. [3]). The valence number of protons (neutrons), N_p (N_n), is defined as the number of particles below midshell and the number of holes past. The $B(E2;0_1^+\rightarrow 2_1^+)$ predictions from this type of systematics are also given in Ref. [3] and those for the xenon isotopes are shown in Fig. 1(d). These values peak at midshell as expected. The underprediction does remain, although not as severely as is the case with the global systematics.

2. Single-shell asymptotic Nilsson model

One of the simplest theoretical models for understanding the $B(E2;0_1^+\rightarrow 2_1^+)$ trends is the SSANM based on the ansatz "A nucleus is as deformed as it can be in a *single* shell."

TABLE I. $B(E2;0_1^+ \rightarrow 2_1^+)$ values for the light Xe ($Z=54$) isotopes.

Nucleus	$E(2_1^+$ state) (keV)	$B(E2;0_1^+ \rightarrow 2_1^+)$ (e^2b^2)	Method	Year[a]	Laboratory	Reference
$^{118}Xe_{64}$	337.0	1.32 ± 0.10	Recoil distance	1977	Strasbourg	[14]
		1.40 ± 0.07	Recoil distance	1980	RIKEN	[15]
		1.43 ± 0.14	Delayed coincidence	1992	UNISOR	[16]
		1.38 ± 0.06	Adopted value			
$^{120}Xe_{66}$	321.8	0.92 ± 0.11	Recoil distance	1972	Heidelberg	[17]
		0.94 ± 0.09	Recoil distance	1980	RIKEN	[15]
		0.94 ± 0.20	Recoil distance	1985	Notre Dame	[18]
		$1.73^b \pm 0.11$	Recoil distance	1985	Köln	[19]
		1.53 ± 0.14	Recoil distance	1990	Köln	[20]
		1.79 ± 0.11	Delayed coincidence	1992	UNISOR	[16]
		1.65 ± 0.31	Recoil distance	1993	Notre Dame	[21]
		1.69 ± 0.09	Adopted value			
$^{122}Xe_{68}$	331.3	1.12 ± 0.10	Recoil distance	1972	Heidelberg	[17]
		2.00 ± 0.20	Recoil distance	1992	VICKSI	[22]
		1.33 ± 0.10	Recoil distance	1993	Köln	[23]
		1.42 ± 0.04	Recoil distance	1994	Köln	[24]
		1.42 ± 0.04	Adopted value			
$^{124}Xe_{70}$	354.1	0.90 ± 0.07	Coulomb excitation	1975	Rutgers	[25]
		$1.49^b \pm 0.09$	Recoil distance	1985	Köln	[19]
		1.19 ± 0.10	Recoil distance	1990	Köln	[20]
		1.00 ± 0.14	Adopted value			

[a]Year in which the results became generally available (see references) and not necessarily the year in which measurements were made.
[b]Preliminary value superseded by the value given in the next row. Not shown in Fig. 1(b).

We have discussed this model at some length in previous papers [5,6]. In the version that we developed in Ref. [6], the $B(E2;0_1^+ \rightarrow 2_1^+)$ values (in units of e^2 b^2) are given by

$$B(E2;0_1^+ \rightarrow 2_1^+) = \frac{5}{16\pi}|Q_0|^2 = (1.02 \times 10^{-5}) A^{2/3} C^2_{\text{model}} [e_\pi Q^v_\pi + e_\nu Q^v_\nu]^2, \quad (5)$$

where the mass quadrupole moments Q^v_π (Q^v_ν) of the valence (v) protons (neutrons) obtained from this (or any other similar) model are in units of the oscillator size parameter $\alpha^2 = \hbar/M\omega = 0.0101A^{1/3}$ b, and the proton (neutron) effective charges e_π (e_ν) are

$$e_\pi = [1 + (Z/A)]e \quad \text{and} \quad e_\nu = \varepsilon(Z/A)e. \quad (6)$$

We recommended the use of $\varepsilon = 2.1$ in the rare-earth and actinide regions. With *this* choice, we obtained best fit to the $B(E2;0_1^+ \rightarrow 2_1^+)$ data in the "tin" region with Eq. (5) and a *single* constant $C_{\text{SSANM}} = 0.80 \pm 0.07$.

For the xenon ($Z=54$) isotopes in the $A = 104-136$ region, the closed core consists of $Z=50$ protons and $N=50$ neutrons. This core is spherical with zero quadrupole moment. We know from universal model calculations (discussed in Sec. III C) that all even-even xenon isotopes in this region (with the possible exception of ^{130}Xe) are most probably prolate. The standard valence shell for this region consists of the $g_{7/2}$, $d_{5/2}$, $h_{11/2}$, $d_{3/2}$, and $s_{1/2}$ single-particle levels. The asymptotically deformed Nilsson states (see Fig. 2) are labeled by the quantum numbers k^π ($k = \langle j_z \rangle$, $\pi =$ parity). In units of $0.0101A^{1/3}$ b, the sequence of mass quadrupole moments

$$q_k = \langle k^\pi | r^2 Y^0_2 | k^\pi \rangle \quad (7)$$

for some of the asymptotic Nilsson states (orbits) in the $50 \leq (Z,N) \leq 82$ region are given in Table IV of Ref. [6]. The complete set of $|k|^\pi(q_k)$ values, in decreasing order of q_k, is $1/2^+(7.4)$, $1/2^+(3.8)$, $3/2^+(3.5)$, $1/2^-(3.2)$, $3/2^-(2.6)$, $5/2^-(1.5)$, $3/2^+(0.2)$, $7/2^-(-0.1)$, $1/2^+(-0.2)$, $5/2^+(-0.2)$, $9/2^-(-2.3)$, $5/2^+(-3.5)$, $1/2^+(-3.7)$, $3/2^+(-3.7)$, $7/2^+(-3.8)$, and $11/2^-(-5.0)$. If we now consider $^{120}_{54}Xe_{66}$ as an example, the maximally deformed

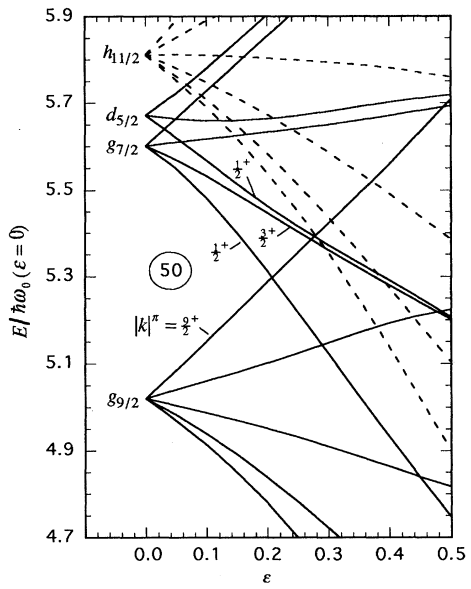

FIG. 2. Selected portion of the single-particle Nilsson level spectrum for protons as a function of deformation.

intrinsic state is obtained by putting four valence protons (two each) in the two $|k|^\pi=1/2^+(g_{7/2})$ and $|k|^\pi=1/2^+(d_{5/2})$ orbits with a total moment of $Q_\pi^v=22.4\alpha^2$, and 16 valence neutrons (two each) in the first eight of the above listed $|k|^\pi$ orbits with a total moment of $Q_\nu^v=44.3\alpha^2$. After taking into account the effective charges $e_\pi=1.45e$ and $e_\nu=0.94e$ [see Eq. (6)], the intrinsic electric quadrupole moment Q_0 is $(0.8)(74.3)\alpha^2 e=2.96\ e$ b, and the $B(E2;0_1^+\rightarrow 2_1^+)$ value from Eq. (5) is 0.87 e^2 b^2. This value and those calculated in a similar fashion for the remaining isotopes are shown in Fig. 1(e). The special characteristic of the calculated $B(E2;0_1^+\rightarrow 2_1^+)$ trend is the flatness at the top—the values for the five xenon isotopes in the $N=62-70$ ($A=116-124$) region are nearly the same. This flatness is an inherent feature of the quadrupole moment spectrum of the single-shell asymptotic Nilsson model. It arises because the moments of the four deformed orbits at the middle of the shell are small and the net quadrupole moment therefore changes very slowly as these orbits are occupied successively. The $B(E2;0_1^+\rightarrow 2_1^+)$ trend for the light xenon isotopes, on the other hand, does not at all show this flat behavior. Moreover, the SSANM seriously underpredicts the values for $^{118}Xe_{64}$, $^{120}Xe_{66}$, and $^{122}Xe_{68}$.

3. MONSTER calculations

Properties of the xenon isotopes have been calculated within the 50–82 major shell by Hammarén *et al.* [26] using the MONSTER model [27]. The effective charges $e_\pi=1.73e$ and $e_\nu=0.73e$ used by them are somewhat different from $e_\pi\approx 1.45e$ and $e_\nu\approx 0.94e$ used by us in Sec. III B 2, but the sum of these two charges is nearly the same in both. The $B(E2;0_1^+\rightarrow 2_1^+)$ values for $^{120}Xe_{66}$, $^{124}Xe_{70}$, and $^{126}Xe_{72}$ predicted by this model are shown in Fig. 1(e). As seen from this figure, neither the simplest (SSANM) nor the most complex (MONSTER) shell-model calculation [restricted to the *single* $50\leqslant(Z,N)\leqslant 82$ shell] reproduces the measured $B(E2;0_1^+\rightarrow 2_1^+)$ trend correctly.

4. Interacting boson approximation

The interacting boson approximation (IBA) provides an economical description of collective states of nuclei. While its connection to underlying fermion dynamics has not yet been fully established, the success of the IBA in correlating a large amount of data is well documented [28]. The two exact symmetries of IBA-1 appropriate for the 50–82 shell are SU(5) for vibrational nuclei and SO(6) for γ-soft rotational nuclei. Deviations from exact symmetry are incorporated into IBA-2 by explicitly diagonalizing the Hamiltonian, whose parameters are determined by simultaneously fitting the energy level spectra for several nuclei in the chosen region. Such an IBA-2 calculation has been carried out for the xenon, barium, and cerium isotopes by Otsuka, Pan, and Arima [29], who also make a strong case for inclusion of the Pauli blocking effects while calculating spectral properties. The resulting $B(E2;0_1^+\rightarrow 2_1^+)$ values of the xenon isotopes are shown in Fig. 1(f). The agreement with experiment is excellent for the $N\geqslant 70$ xenon isotopes, for which the dominant symmetry is SU(5). However, for the more deformed midshell xenon isotopes, whose dominant symmetry should be SO(6), there is a marked underprediction. Because the majority of the fitted energy levels belong to SU(5) nuclei, the Hamiltonian might not be representative enough for the entire region, thereby leading to underpredictions for SO(6) nuclei. Ironically, the IBA-2 predictions without the Pauli blocking factors, shown in Fig. 4(a) of Ref. [29], are in good agreement with the new data for the lighter xenon isotopes.

5. Fermion dynamic symmetry model

The fermion dynamic symmetry model (FDSM) [30] is, in principle, capable of carrying out a complete shell-model calculation in a given shell. However, the usefulness of this model derives, as for the IBA, from its economic description of the collective states of nuclei in terms of different symmetry limits (see, for example, Fig. 4 of Ref. [5] pertaining to the 82–126 region). The exact limiting symmetries for the i-active 50–82 shell nuclei are SO(7) (vibrational) and SO(6) (rotational). A FDSM calculation that allows for mixing of these symmetries has not been reported. The $B(E2;0_1^+\rightarrow 2_1^+)$ values in the SO(6) limit will be shown later, but those in the SO(7) limit [31] are shown in Fig. 1(f). The FDSM results without symmetry mixing are nearly the same as the IBA-2 results with Pauli blocking and symmetry mixing. The peak in the $B(E2;0_1^+\rightarrow 2_1^+)$ values for the midshell xenon isotopes remains to be explained.

C. Universal systematics

Several powerful models (which require elaborate computer programs) have been developed that determine the equilibrium shapes of the lowest-energy intrinsic states of several thousand nuclei between the proton and neutron drip lines. Because these models include all nucleons explicitly in the calculation, they do not need effective charges for calculating the $B(E2;0_1^+\rightarrow 2_1^+)$ values. All of these models mini-

mize the total energy of the intrinsic state to fix the parameters of the model. The intrinsic state is described by

$$r(\theta,\phi)=R_0[1+\beta_2 Y_2^0(\cos\theta)+\beta_4 Y_4^0(\cos\theta)+\cdots]. \quad (8)$$

The β_2 and β_4 values for the equilibrium shape determine the intrinsic quadrupole moment by the relation [32]

$$Q_0=\frac{3}{\sqrt{5\pi}}ZR_0^2\left(\beta_2+\frac{2}{7}\sqrt{5/\pi}\beta_2^2+\frac{20}{77}\sqrt{5/\pi}\beta_4^2+\frac{12}{7\sqrt{\pi}}\beta_2\beta_4\right)+O(\beta^3). \quad (9)$$

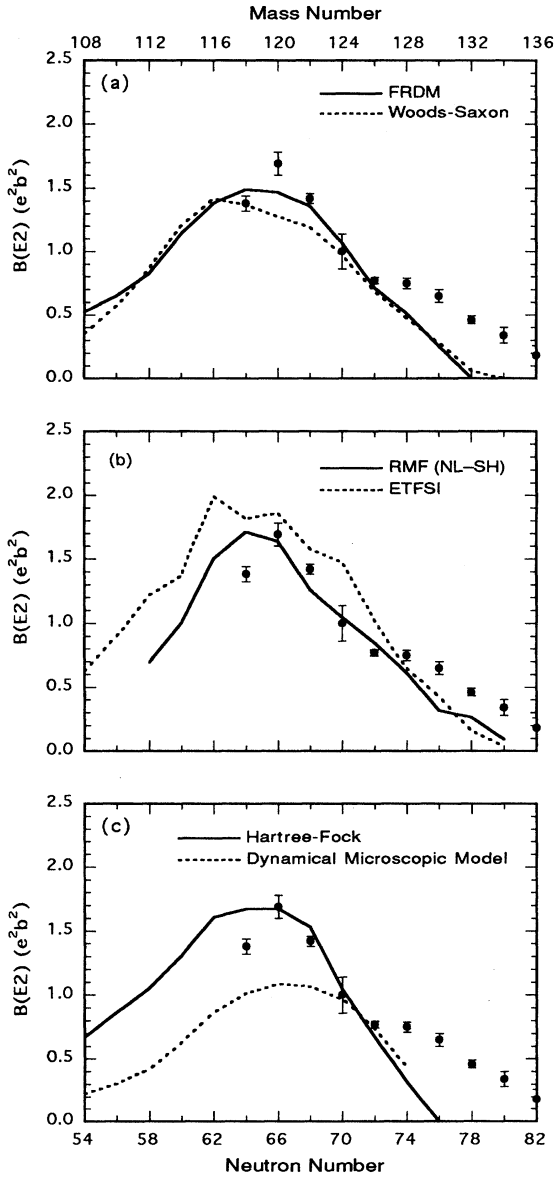

FIG. 3. Comparison between measured and calculated $B(E2;0_1^+\rightarrow 2_1^+)$ values of even-even xenon isotopes. Measured values shown are those adopted in Table I. Various curves refer to universal models discussed in Sec. III C.

The $B(E2;0_1^+\rightarrow 2_1^+)$ value is then given by

$$B(E2;0_1^+\rightarrow 2_1^+)=\frac{5}{16\pi}|Q_0|^2. \quad (10)$$

The uncertainty in the deduced deformation depends, say, on the sharpness of the total energy vs deformation curve—some are narrow and some are relatively flat. As a general rule, the uncertainties in the predicted $B(E2;0_1^+\rightarrow 2_1^+)$ values should not exceed 20% and the relative trend should be much better.

In Fig. 3 we show results for the xenon isotopes given by these models. Because these models (with one exception) deal with *static* properties (neglecting shape fluctuations), the $N\geq 74$ tail of the $B(E2;0_1^+\rightarrow 2_1^+)$ trend is not predicted well by these models. In this section, the comparison between theory and experiment is focused on the $B(E2;0_1^+\rightarrow 2_1^+)$ values for the midshell xenon isotopes. Most of the universal models reproduce the new experimental data.

1. Finite-range droplet model (FRDM)

In the FRDM [33] the nuclear ground-state shapes are calculated by minimizing the nuclear potential energy function with respect to ε_2, ε_3, ε_4, and ε_6 shape degrees of freedom in Nilsson's perturbed-spheroid parametrization. The nuclear potential energy of deformation is calculated by use of the macroscopic-microscopic method [34], with the macroscopic contribution calculated from a finite-range droplet model and the microscopic shell and pairing corrections from a folded-Yukawa single-particle potential. Strutinsky's method [35] is used for the shell correction, and the Lipkin-Nogami [36] extension of the BCS method for the pairing correction. The β_2 and β_4 values given by this model for $\sim$9000 nuclei have recently become available [37]. The $B(E2;0_1^+\rightarrow 2_1^+)$ values [deduced from β_2 and β_4 using Eqs. (9) and (10)] for the xenon isotopes are shown in Fig. 3(a). They peak near midshell. Except for $^{120}Xe_{66}$, the overall agreement with experimental data is quite good.

2. Woods-Saxon model

In this model [38], the nuclear ground-state shapes are calculated using Strutinsky's shell-correction method [35]. The macroscopic part of the total energy is assumed to be given by the Yukawa-plus-exponential mass formula [34], and the shell correction is computed using the axially deformed single-particle Woods-Saxon potential [38] with parameters from Ref. [39]. The total energy is minimized with respect to the shape parameters β_2, β_4, and β_6. As in the case of the FRDM, an approximate particle number projection is implemented by means of the Lipkin-Nogami method [36] with pairing strengths from Ref. [33] to evaluate the pairing correction term. The calculated β_2 and β_4 values for $\sim$1400 even-even nuclei using this model have now become available [40], and the deduced $B(E2;0_1^+\rightarrow 2_1^+)$ values for the xenon isotopes are shown in Fig. 3(a). They peak prematurely, and there is some underprediction.

3. Relativistic mean-field (RMF) calculations

Recently, the RMF [41] approach is finding wider use in the description of the ground-state properties of nuclei throughout the periodic table. The basic ingredients in this approach are baryons and mesons. In the current version, the mesons used are the scalar σ, vector ω, and isovector-vector ρ. The Lagrangian density is constructed with these basic degrees of freedom and the equations of motion are derived using the variational ansatz. This procedure results in the Dirac equation for the baryons and the Klein-Gordon equations for the mesons and for the photons with source terms. Charge conservation and time-reversal symmetry are used to reduce the number of equations to be solved self-consistently. The basis expansion method [42] is used to solve the resulting equations of motion. The large and small components of the Dirac spinors and meson fields are expanded in terms of the eigenfunctions of the deformed axially symmetric oscillator potential. The pairing interaction, known to be important for open-shell nuclei, is solved using the constant gap approximation [43].

In generating the average nuclear potential, the use of meson exchange potentials in the RMF is a substantial improvement over the use of Yukawa potentials in the FRDM and the Woods-Saxon model. In particular, the vector meson exchange generates the spin-orbit interaction in a self-consistent way. The strength of this interaction relative to the central potential determines the sequence and spacing of single-particle states. In most other approaches (Hartree-Fock, for instance) this strength is determined from the known spin-orbit splitting. The RMF approach is expected to be more reliable in making predictions for nuclei far from stability [44].

In this work, we have performed numerous RMF calculations. We used 12 oscillator shells for both the Dirac spinors and the meson fields. The spacing between the shells is given by $\hbar\omega = 41A^{-1/3}$ MeV. To check the sensitivity of the results on the parameters of the Lagrangian density, we performed calculations with three different sets of parameters. One of the earliest sets was obtained by Horowitz and Serot (H-S) [45]. In a later formulation, Reinhard *et al.* [46] adjusted the eight parameters of the RMF model to obtain a least-squares fit to the binding energies, radii, and diffuseness of eight stable nuclei. This set, labeled NL1, has been used extensively [42,47], including recently to describe the properties of neutron-rich zirconium and neutron-poor barium isotopes [48]. However, it was pointed out by Sharma, Nagarajan, and Ring [49] that the NL1 set gave incorrect (too large) neutron radii and the NL-SH set was developed to cure this problem. The results obtained for the xenon isotopes using the NL-SH set have been published [49,50]. The $B(E2;0_1^+ \rightarrow 2_1^+)$ values deduced from the β_2 values given in Ref. [49] are shown in Fig. 3(b). They peak at $A = 118$ instead of at $A = 120$; otherwise the agreement with experiment is good.

4. Extended Thomas-Fermi Strutinski-integral (ETFSI) method

In this method, axial and left-right symmetry are assumed, and the deformations are expressed in terms of the (β_2, β_4) coefficients of a multipole expansion of a surface of constant density. The calculations are performed using the ETFSI approximation [51] to the Hartree-Fock (HF) method for Skyrme-type forces, an approximation which consists in first making the extended Thomas-Fermi (ETF) approximation to the HF method, and then adding Strutinsky shell corrections in the integral form (SI), along with BCS pairing corrections based on a δ function force. The ETFSI approximation is equivalent to the HF method in the sense that, when the underlying force is fitted to the same data by one method or the other, the two methods give very similar extrapolations out to the neutron drip line, the disagreement for total masses being <1 MeV [51]. The deformation parameters minimize the total energy (after projecting out the spurious rotational energy) as computed with the parametrization SkSC4 of the Skyrme force. This force, which has just eight active parameters, fits the ~ 1500 known masses in the $36 \leq A \leq 300$ interval with a root-mean-square (rms) error of ~ 740 keV [51]. Using the ETFSI method, the ground-state deformations of ~ 7000 nuclei with $10 \leq Z \leq 130$ and $36 \leq A \leq 300$ have been calculated recently [52]. Some of these nuclei lie beyond the proton and neutron drip lines. The deduced $B(E2;0_1^+ \rightarrow 2_1^+)$ values for the xenon isotopes are shown in Fig. 3(b). They peak prematurely, and there is some overprediction.

5. Hartree-Fock calculations

In these calculations, the nuclear ground-state wave functions are obtained in the framework of the Hartree-Fock plus BCS method [53]. The Skyrme SIII force is used to construct the Hartree-Fock potential, while the seniority force is chosen as the pairing interaction, whose strength is determined such that the empirical average gap $12A^{-1/3}$ MeV is reproduced with the Thomas-Fermi level density. The single-particle wave functions are expressed on a Cartesian mesh of size 1 fm. The number of mesh points is $13 \times 13 \times 14$. An octant of a nucleus is placed in a corner of this box, imposing reflection symmetries (D_{2h}). Total binding energies are corrected for error due to finite mesh size. The results for ~ 880 nuclei using this model have just become available [54]. Those for the xenon isotopes are shown in Fig. 3(c). The $B(E2;0_1^+ \rightarrow 2_1^+)$ values peak at midshell, but the distribution at the peak is again relatively flat. Except for $^{118}Xe_{64}$, the overall agreement with experiment is good.

6. Dynamical microscopic model

This model is based on the generator coordinate method (GCM) with Gaussian overlap approximation [55]. The potential energy of a nucleus is calculated by the shell-correction method of Strutinsky [34] with liquid droplet macroscopic part and zero-point energy. The modified Nilsson single-particle potential is used. The GCM collective Hamiltonian in the two-dimensional (β_2, β_4) space is diagonalized in the harmonic oscillator base. The mean square radii and electric quadrupole moments of ~ 880 nuclei in the $20 \leq Z \leq 98$ region have been recently calculated [56]. The $B(E2;0_1^+ \rightarrow 2_1^+)$ values for the xenon isotopes are shown in Fig. 3(c). Those for $^{118}Xe_{64}$, $^{120}Xe_{66}$, and $^{122}Xe_{68}$ are significantly lower than the data.

IV. REGIONAL MODELS RECONSIDERED

The apparent success of universal models in correctly reproducing the $B(E2;0_1^+ \rightarrow 2_1^+)$ trends near midshell prompts

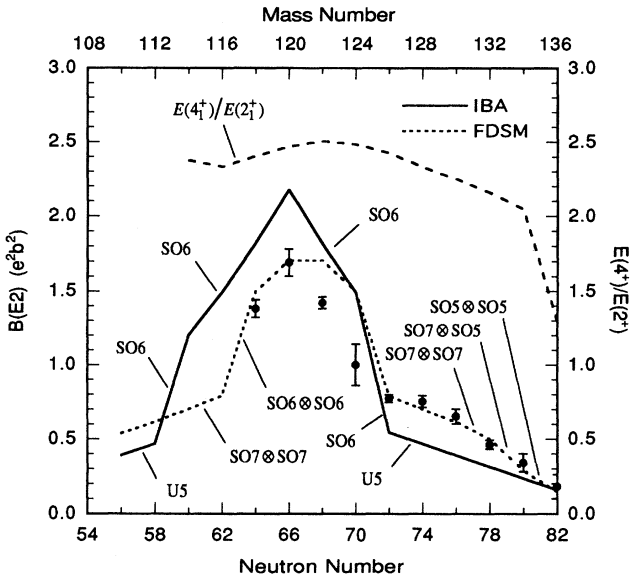

FIG. 4. Comparison between measured $B(E2;0_1^+\rightarrow 2_1^+)$ values of even-even xenon isotopes and those calculated with algebraic models. Various segments of the theoretical curves are calculated assuming the listed limiting symmetries. Also shown (by dashed line) is the ratio of the first 4^+ and the first 2^+ level energies.

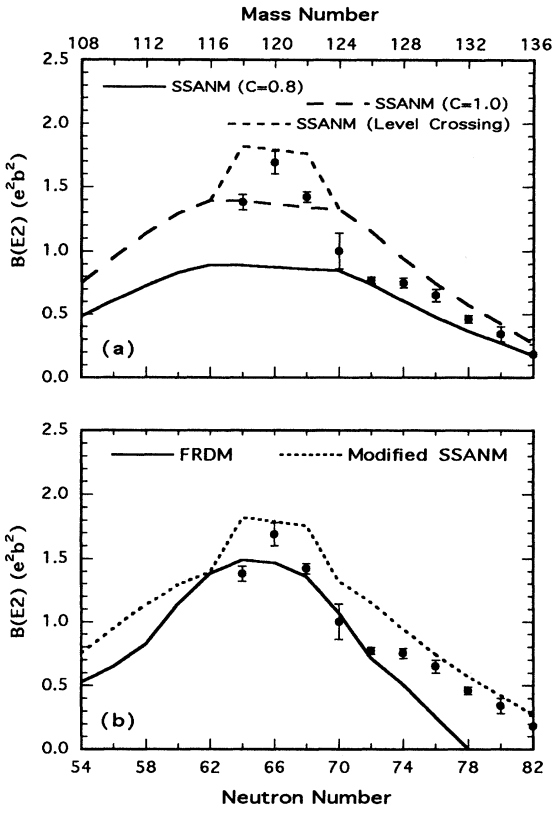

FIG. 5. (a) Measured $B(E2;0_1^+\rightarrow 2_1^+)$ values for the xenon isotopes compared with predictions of the single-shell asymptotic Nilsson model (SSANM). The original SSANM results are modified by changing the normalization C_{model} and by assuming that two protons from the $|k|^\pi=9/2^+(g_{9/2})$ orbit are transferred (with 50% probability) to the $|k|^\pi=3/2^+(g_{7/2})$ orbit because of level crossing. (b) Comparison of the finite-range droplet model (FRDM) and modified SSANM predictions with experiment.

us to reexamine the global and regional models which failed to do so to varying degrees. Based as it is on $B(E2;0_1^+\rightarrow 2_1^+)$ data for even-even nuclei throughout the period table, the global systematics given by Eq. (1) is relatively immutable. Therefore, any disagreement with new data must be ascribed to the deficiencies of this model. Predictions based on the regional $\beta_2'/\beta_{2(sp)}'$ fit may improve when the "tin" region is reanalyzed later as more data become available at midshell. A new MONSTER calculation which relaxes the single-shell constraint and explicitly includes the $1g_{9/2}$ orbit in the model space would be of interest but is beyond the scope of this work. We now reexamine the remaining models discussed in Sec. III B.

A. Algebraic models

The algebraic models have flexibility concerning group classification that affects the predictions. Ideally, there should be some experimental indicators, such as the ratio $E(4_1^+)/E(2_1^+)$, which suggests when a group change should occur corresponding to a first-order phase change from vibrational to rotational behavior. This ratio is relatively flat for the xenon isotopes (see the dashed curve in Fig. 4) except near the $N=82$ closed shell. Nevertheless, as calculated by Wu [31] and shown in Fig. 4, predictions can be made with appropriate group changes that bring the FDSM predictions into good agreement with experiment. The IBA predictions shown in Fig. 4 are those supplied by Wu [31]. They correspond to the indicated limiting symmetries and do not include any Pauli factors. In both models, the dramatic increase in the $B(E2;0_1^+\rightarrow 2_1^+)$ values for midshell xenon isotopes (see Fig. 4) results mainly from the increase in the contribution made by the neutrons. Inclusion of the Pauli blocking effects in the IBA should bring its predictions closer to the FDSM predictions and to the experimental data. However, proponents of both algebraic models will be hard pressed to simultaneously account for the $B(E2;0_1^+\rightarrow 2_1^+)$ trend and level systematics (see, for example, Fig. 2 of Ref. [29]).

B. Single-shell asymptotic Nilsson model

1. Renormalization

In Refs. [5,6] we showed that the SSANM reproduces the measured $B(E2;0_1^+\rightarrow 2_1^+)$ values reasonably well in the $50\leq Z\leq 82$, $82\leq N\leq 126$ (rare-earth) and $82\leq Z\leq 126$, $126\leq N\leq 184$ (actinide) regions. If we assume that the effective charges are given correctly by Eq. (6), this model has one adjustable parameter C_{SSANM} in each region [see Eq. (5)] which we determined by least-squares fits to the data in that region. There are only ~ 30 data points in the actinide region but they follow smooth trends. With ~ 90 data points, the rare-earth region is the best studied region in the periodic

table. In these two regions, the C_{SSANM} values are 1.00 ± 0.04 and 1.01 ± 0.08, respectively; that is, no normalization is required at all in these regions. By contrast, in the "tin" region under study, there are ~ 40 data points but they are clustered mostly near the $N=82$ end. In particular, data near $N=66$ (midshell) are conspicuously absent. Therefore, the C_{SSANM} value 0.80 ± 0.07 for this region is not well determined.

There are esthetic reasons to select $C_{\mathrm{SSANM}}\approx 1.00$ for the "tin" region also, thus making the SSANM on par in all three regions with the same normalization and prescription for effective charges. As shown in Fig. 5(a), agreement with the xenon data at midshell is significantly improved with this renormalization. Moreover, the peak values at midshell are now comparable, as shown in Fig. 5(b), for the SSANM and FRDM.

2. Level crossing

We return to the Nilsson diagram of Fig. 2. According to the SSANM of Sec. II B 2, the 50 protons of the xenon ($Z=54$) isotopes constitute a closed core, and the four valence protons occupy the $|k|^{\pi}=1/2^{+}(g_{7/2})$ and $1/2^{+}(d_{5/2})$ orbits. We note that at $\varepsilon\approx 0.28$ ($\beta_2\approx 0.30$) the occupied $9/2^{+}(g_{9/2})$ upward-sloping (oblate) orbit crosses the empty down-sloping (prolate) $3/2^{+}(g_{7/2})$ orbit. We can now imagine a pairwise proton transfer taking place (either fully or partly) from the oblate to the prolate orbit. If selectively applied to $^{118}\mathrm{Xe}_{64}$, $^{120}\mathrm{Xe}_{66}$, and $^{122}\mathrm{Xe}_{68}$, and if the transfer probability is 100%, this mechanism will boost the proton quadrupole moment by $-(-8\alpha^2)$ corresponding to holes in the $9/2^{+}$ oblate orbit and $+7\alpha^2$ to particles in the newly occupied $3/2^{+}$ prolate orbit. This gain is in addition to $22.4\alpha^2$ already present bringing the grand total to $37.4\alpha^2$. [This total would remain the same if the four valence protons went initially into the $1/2^{+}(g_{7/2})$ and $3/2^{+}(g_{7/2})$ orbits—which is possible because they have very similar asymptotic quadrupole moments—and the transfer took place to the $1/2^{+}(d_{5/2})$ orbit.] For a 50% transfer probability, the proton quadrupole moment would be $29.9\alpha^2$. With this assumption, the resulting $B(E2;0_1^{+}\rightarrow 2_1^{+})$ values are shown in Figs. 5(a) and 5(b). There is thus a natural mechanism in the SSANM that can produce a peak if it is warranted. This mechanism, unlike the case with the algebraic models, now involves the protons.

3. Justifying the changes in SSANM

According to the SSANM, the most deformed nucleus in the "tin" region would be $^{128}_{64}\mathrm{Gd}_{64}$. The $B(E2;0_1^{+}\rightarrow 2_1^{+})$ trend for the gadolinium isotopes with $C_{\mathrm{SSANM}}=0.80$ in the "tin" region is shown by the dashed line in Fig. 6. Also shown (solid line) is the trend predicted by the FRDM. At $N=64$, the SSANM value is less than half of the FRDM value. We can reduce this discrepancy by choosing $C_{\mathrm{SSANM}}=1.0$ for the "tin" region (see dotted line in Fig. 6) just as it is for the rare-earth and actinide regions. With this choice, the existing agreement with the *limited* $B(E2;0_1^{+}\rightarrow 2_1^{+})$ data near the $N=82$ end would suffer, but only slightly. Therefore the proposed change is justified at this time pending a later determination of the best values of

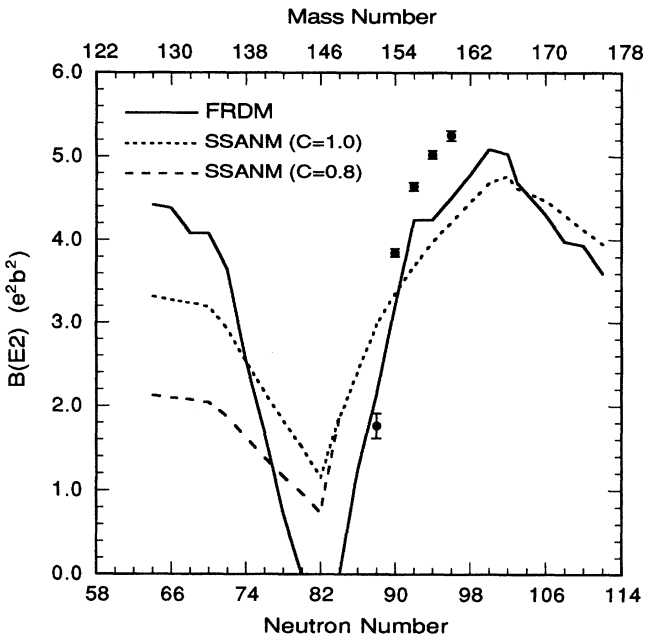

FIG. 6. Calculated and measured $B(E2;0_1^{+}\rightarrow 2_1^{+})$ values for the gadolinium ($Z=64$) isotopes. Beyond $N=82$, $C_{\mathrm{model}}=1.0$ in the SSANM. Measured $B(E2;0_1^{+}\rightarrow 2_1^{+})$ values shown are those adopted in Ref. [1].

C_{SSANM} and effective charges for the "tin" region as more data become available at midshell.

4. Level occupancies

Before considering the implications of level crossings, we take one of these models—the relativistic mean-field (RMF) model with which an extensive set of predictions is not yet available—and show how sensitive the results are to input parameters. The RMF results connected by solid lines in Figs. 3(b) and 7(a) uses the NL-SH set of parameters [49] and theoretical neutron and proton pairing gaps given by $\Delta_n=\Delta_p=12A^{-1/2}$ MeV [57]. We have repeated these calculations with experimental gaps (given by Eqs. 2–92 and 2–93 of Ref. [57]). The results are significantly different as shown by the dotted line in Fig. 7(a). The maximum has shifted from $N=64$ to $N=66$ and the peak at midshell has become sharper, both in better agreement with the data.

The $B(E2;0_1^{+}\rightarrow 2_1^{+})$ values that we calculated with the H-S, NL1, and NL-SH sets of parameters (and experimental pairing gaps) are compared with measurements in Fig. 7(b). Also shown in Fig. 7(c) are predictions of the Woods-Saxon model. The increase in deformation for $^{118}\mathrm{Xe}_{64}$, $^{120}\mathrm{Xe}_{66}$, and $^{122}\mathrm{Xe}_{68}$ is very dramatic [see Fig. 7(b)] using the NL1 set. These predictions are not supported by the data. This is one more example of why the NL-SH set is preferable over NL1. For our purposes, however, this gross overprediction is fortuitous because we can use this result to trace the detailed behavior of the level occupancies.

Figures 8(a), 8(c), and 8(e) show the changing positions of several single-particle levels (for protons) relative to the $|k|^{\pi}=7/2^{-}(h_{11/2})$ level which lies relatively flat for the xe-

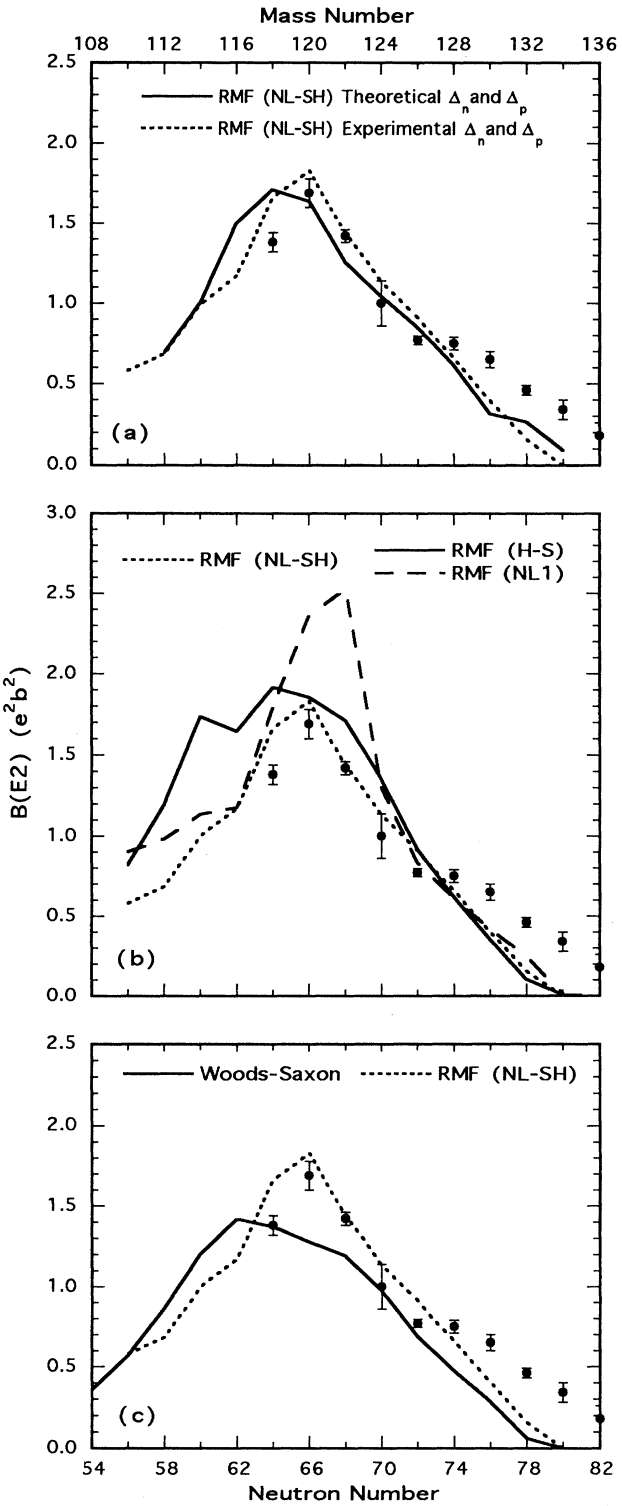

FIG. 7. Changes in $B(E2;0_1^+\rightarrow 2_1^+)$ values for the xenon isotopes given by the relativistic mean-field (RMF) calculations with (a) the same set of model parameters (NL-SH) but differing prescriptions for pairing gaps and (b) the same experimental pairing gaps but differing set of model parameters (H-S, NL-SH, and NL1). (c) Comparison of the Woods-Saxon and RMF (NL-SH) predictions with experiment.

non isotopes (see Fig. 2). The single-particle spectrum is more compressed with the Woods-Saxon than with either the RMF (NL-SH) or RMF (NL1). With the NL1 set, the $9/2^+(g_{9/2})$ level, after crossing the $1/2^+(g_{7/2})$ level, comes very close, around midshell [see Fig. 8(e)], to the $3/2^+(g_{7/2})$ and $1/2^+(d_{5/2})$ levels. This proximity is reflected in the calculated occupancies [see Fig. 8(f)] which show a corresponding depletion of the $9/2^+(g_{9/2})$ orbit and increased occupancies of the $3/2^+(g_{7/2})$ and $1/2^+(d_{5/2})$ orbits. The sharp peak (for NL1) in Fig. 7(b) is a direct result of these changing occupancies. A similar behavior is what we put in by hand when modifying the SSANM in Sec. IV B 2.

An apparent peak in the $B(E2;0_1^+\rightarrow 2_1^+)$ vs N curve can be a result of an increase at the apex or a decrease in the wings or both. The relevant levels do not come as close together at midshell with the NL-SH set [see Fig. 8(c)] as with the NL1 set [Fig. 8(e)]. Therefore, a pronounced depletion of the $9/2^+(g_{9/2})$ orbit is not indicated in Fig. 8(d) at $N\approx 66$. However, at $N=62$, there is now a noticeable decrease in the occupancies of both $1/2^+(g_{7/2})$ and $3/2^+(g_{7/2})$ orbits (with large positive quadrupole moments) and corresponding increases in all other orbits (with negative moments or smaller positive moments). Consequently, there is a steeper decrease in the $B(E2;0_1^+\rightarrow 2_1^+)$ value [see the dotted NL-SH curve corresponding to experimental pairing gaps in Fig. 7(a)] when going from $N=64$ to $N=62$ compared to the more gradual drop when going from $N=66$ to $N=64$ or from $N=62$ to $N=60$. The net result is the appearance of a small peak [for NL-SH (experimental gaps)] at $N\approx 66$ in Fig. 7(a). The behavior of the occupancies at $N=62$ can be traced to the high values, $\Delta_n=2.130$ and $\Delta_p=1.930$ MeV, of the experimental pairing gaps for $^{116}_{54}Xe_{62}$. These gaps, which are nearly twice the theoretical gaps, are the largest for an even-even xenon nucleus in the $A=110-136$ region.

The separation between the $9/2^+(g_{9/2})$ level and remaining levels [see Fig. 8(a)] changes more gradually in the Woods-Saxon model than in the RMF model. Consequently the occupancies change more slowly in the former model and the $B(E2;0_1^+\rightarrow 2_1^+)$ trend [see Fig. 7(b)] is broader. Moreover, the $1/2^-(h_{11/12})$ level descends below the $3/2^+(g_{7/2})$ level at $N=60$ and stays below until $N=64$. As a result, the occupancy of the $1/2^-(h_{11/12})$ level shows a significant increase [see Fig. 8(b)] reaching a maximum at $N=62$. The resulting $B(E2;0_1^+\rightarrow 2_1^+)$ trend also peaks at $N=62$ [see Fig. 7(c)], which is four nucleons below midshell.

Even though the final calculated deformation in these three calculations are similar, Fig. 8 clearly shows that the behavior of the single-particle energies and occupancies are quite different.

V. DEFORMATION OF BARIUM ISOTOPES

The $B(E2;0_1^+\rightarrow 2_1^+)$ values of the rare-earth nuclei in the $50\leq Z\leq 82$, $82\leq N\leq 126$ region peak at (or very close to) midshell (see Fig. 10 of Ref. [5]). Whether a similar behavior occurs in the $50\leq (Z,N)\leq 82$ region is unknown at this time because the required data do not exist. However, some of the universal models predict (see Fig. 9) that the peak for the barium isotopes will occur at $N\approx 60$ or $N\approx 62$, well below the midshell value of $N=66$. Lifetime data for the 2_1^+ states

of $^{122}_{56}Ba_{66}$ and $^{124}_{56}Ba_{68}$ have appeared recently [58,23], but the $B(E2;0_1^+ \rightarrow 2_1^+)$ value of 1.35 ± 0.12 e^2 b^2 obtained by Morikawa *et al.* [58] for $^{124}_{56}Ba_{68}$ is badly discrepant with 1.99 ± 0.08 e^2 b^2 obtained by Sala [23]. (In Fig. 9 we have shown the latter value.) As more data become available for the lighter barium isotopes (and for the cerium, neodymium, and samarium isotopes as well) and are confirmed, they will pose a stringent test for theoretical models and systematics.

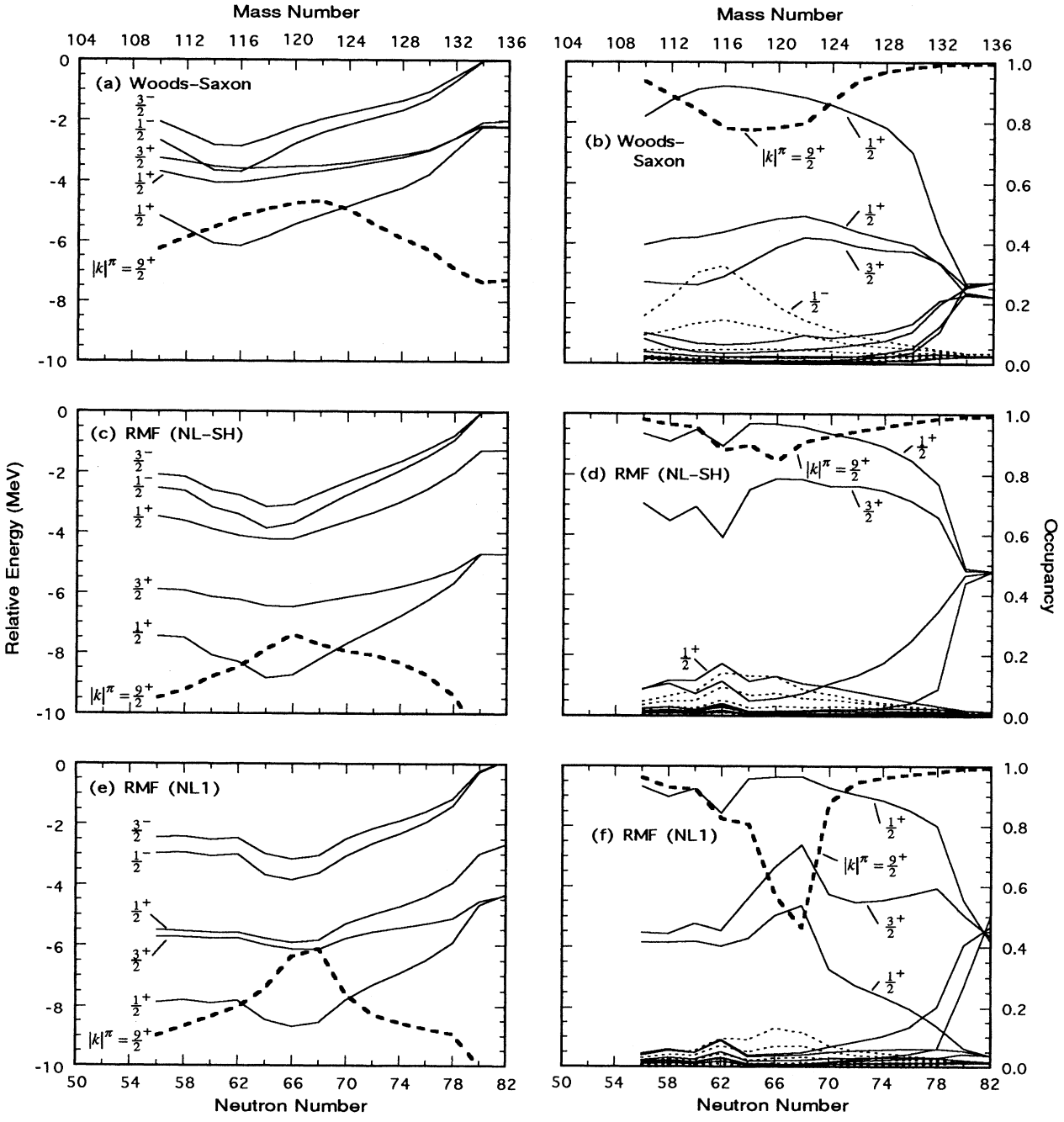

FIG. 8. Results for the xenon isotopes given by the Woods-Saxon and relativistic mean-field (RMF) models, the latter with two different sets of model parameters (NL1 and NL-SH). Energies of selected single-particle levels relative to the $|k|^\pi = 7/2^-(h_{11/2})$ level are shown in (a), (c), and (e). Occupancies of all 16 orbits pertaining to the $50 \leq Z \leq 82$ region and the occupancy of the $|k|^\pi = 9/2^+(g_{9/2})$ orbit from the lower region are shown in (b), (d), and (f). Occupancies of abnormal-parity states are shown by dotted lines. Full occupancy corresponds to 1.0.

VI. CONCLUSIONS

In a previous paper [5], we showed that a variety of models with very different starting points, assumptions, and calculational difficulties are all capable of reproducing the overall $B(E2;0_1^+\rightarrow 2_1^+)$ trends in the rare-earth and actinide regions in a satisfactory manner. All models have adjustable parameters, stated or unstated, built into them and empirical models especially require experimental $B(E2;0_1^+\rightarrow 2_1^+)$ data to reciprocally reproduce such data. Just because of this requirement, such models should not be overlooked. On the

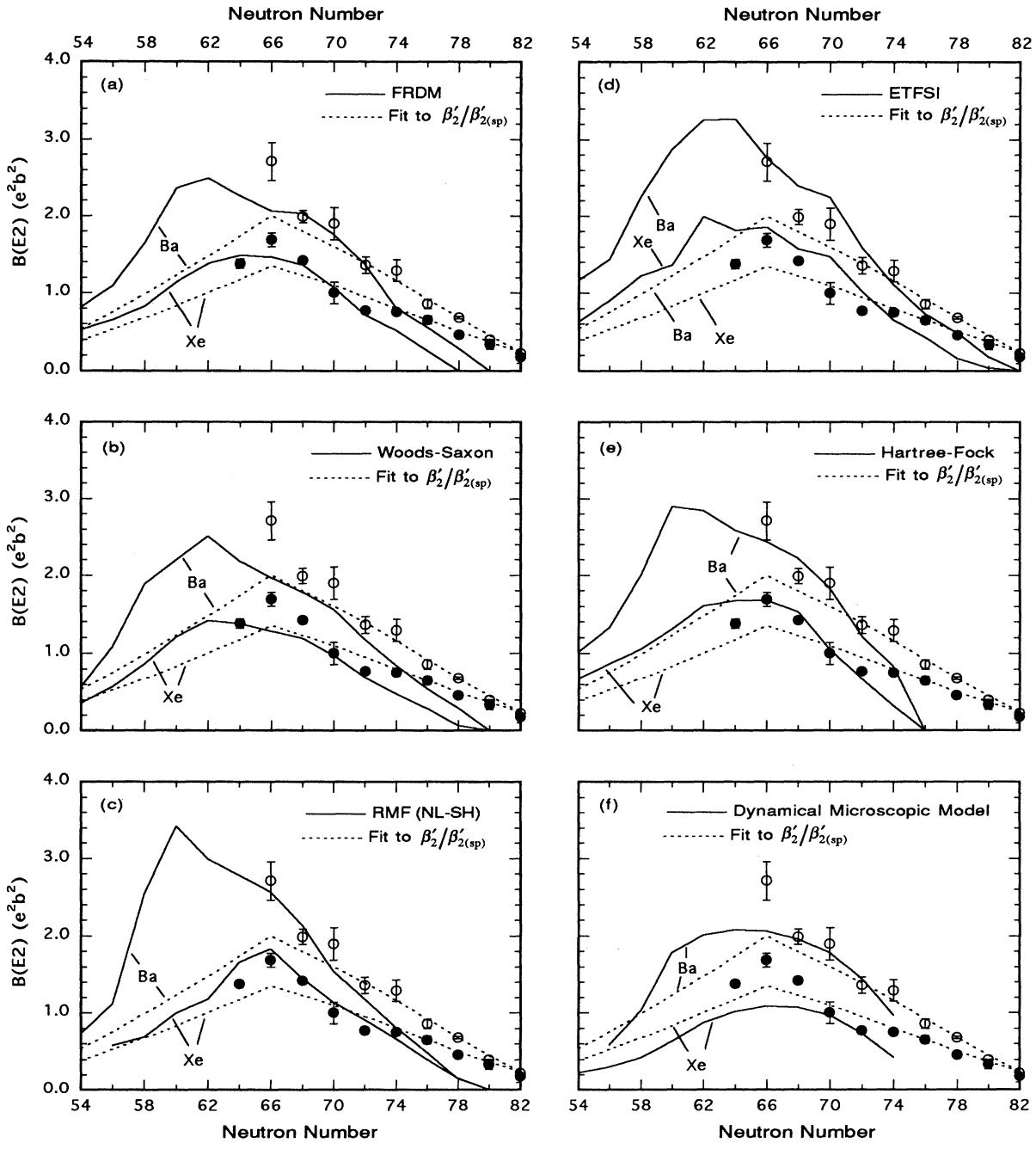

FIG. 9. Comparison between measured and calculated $B(E2;0_1^+\rightarrow 2_1^+)$ values of even-even xenon and barium isotopes. Closed circles refer to the xenon data, open circles to the barium. The different models are discussed in Sec. III. The RMF (NL-SH) results shown in (c) are based on experimental pairing gaps. The measured $B(E2;0_1^+\rightarrow 2_1^+)$ values for $^{122}_{56}Ba_{66}$ and $^{124}_{56}Ba_{68}$ are from Refs. [58] and [23], respectively. Remaining values are those recommended in Ref. [1].

countervailing side, they are simple, physically intuitive, and capable of answering or anticipating many questions. Empirical predictions tend to be structureless compared to either the predictions of more sophisticated models or experimental data. It is important to understand these structures (peaks, wiggles, dips, etc.). If they are real, it may be possible to find clues about their origin even with simple models.

In the $50 \leq (N,Z) \leq 82$ ("tin") region, empirical models apparently fare poorly. The adopted $B(E2;0_1^+ \rightarrow 2_1^+)$ value of ${}^{120}_{54}Xe_{66}$ is higher than either the maximum value predicted by the simple SSANM (with $C_{\mathrm{SSANM}}=1.0$) or the value given by the more complex MONSTER shell-model calculations. The rapid rise of the $|k|^{\pi}=9/2^+(g_{9/2})$ oblate orbit for protons as a function of deformation and its intrusion into the 50–82 shell suggest a simple mechanism for increasing the $B(E2;0_1^+ \rightarrow 2_1^+)$ value as a result of partial emptying of this orbit due to pairing.

There can be other mechanisms as well. In the IBA and FDSM, it can be argued that the $B(E2;0_1^+ \rightarrow 2_1^+)$ variations indicate a first-order phase transition from a vibrational symmetry [U(5) or SO(7)] to rotational symmetry [SO(6)]. Here the instigators are the neutrons. However, there is no evidence for such a phase transition from the level energies.

The universal models, which are fairly successful in explaining these $B(E2;0_1^+ \rightarrow 2_1^+)$ values, do not have much to say about the level spectra. The emptying of the $9/2^+(g_{9/2})$ orbit does play a role in some of the universal models, but the detailed manner by which the midshell xenon isotopes acquire significant deformation is more complex. Even though the parameters of the universal models are fixed very early in the calculations and the $B(E2;0_1^+ \rightarrow 2_1^+)$ predictions are firm and predetermined, these parameters, too, are subject to refinements. It is axiomatic that these models should be reexamined often as more data [not only $B(E2;0_1^+ \rightarrow 2_1^+)$ values but also masses, mean square radii, position of the drip lines, etc.] become available and the results are subjected to detailed comparisons such as those carried out in this work.

Providing a consistent explanation for the significant increase in the $B(E2;0_1^+ \rightarrow 2_1^+)$ values of the midshell xenon isotopes *without* a concomitant change in the energies of low-lying states is a new challenge facing nuclear models.

ACKNOWLEDGMENTS

We thank C. -L. Wu, P. Möller, J. R. Nix, T. R. Werner, J. M. Pearson, H. Tajima, B. Nerlo-Pomorska, and K. Pomorski for providing us with the theoretical results and for clarifying details about their respective calculations. Even though the RMF results obtained by D. Hirata and H. Toki were not actually used in this paper, they revealed considerable sensitivity of the RMF results to input parameters. We also thank P. F. Mantica, U. Garg, and A. Dewald for sharing the new experimental results. Nissan Zeldes and Murray Martin read the manuscript critically. The current work was sponsored by the U. S. Department of Energy under Contract No. DE-AC05-84OR21400 with Martin Marietta Energy Systems, Inc. Two of the authors (J. A. S. and K. H. B.) were supported in part by the Joint Institute of Heavy-Ion Research. This institute is supported by the U. S. Department of Energy under Contract No. DE-AS05-76ERO-4936 with The University of Tennessee and is operated jointly by The University of Tennessee, Vanderbilt University, and Oak Ridge National Laboratory.

[1] S. Raman, C. H. Malarkey, W. T. Milner, C. W. Nestor, Jr., and P. H. Stelson, At. Data Nucl. Data Tables **36**, 1 (1987).
[2] S. Raman, C. W. Nestor, Jr., and K. H. Bhatt, Phys. Rev. C **37**, 805 (1988).
[3] S. Raman, C. W. Nestor, Jr., S. Kahane, and K. H. Bhatt, At. Data Nucl. Data Tables **42**, 1 (1989).
[4] S. Kahane, S. Raman, and J. Dudek, Phys. Rev. C **40**, 2282 (1989).
[5] S. Raman, C. W. Nestor, Jr., S. Kahane, and K. H. Bhatt, Phys. Rev. **43**, 556 (1991).
[6] K. H. Bhatt, C. W. Nestor, Jr., and S. Raman, Phys. Rev. C **46**, 164 (1992).
[7] S. Raman, Rev. Mex. de Fis. **39**, Supplemento 2, 201 (1993).
[8] K. H. Bhatt, C. W. Nestor, Jr., and S. Raman, Phys. Rev. C **49**, 808 (1994).
[9] M. N. Rao, N. R. Johnson, F. K. McGowan, I. Y. Lee, C. Baktash, M. Oshima, J. W. McConnell, J. C. Wells, A. Larabee, L. L. Riedinger, R. Bengtsson, Z. Xing, Y. S. Chen, P. B. Semmes, and G. A. Leander, Phys. Rev. Lett. **57**, 667 (1986).
[10] S. Raman, C. W. Nestor, Jr., S. Kahane, and K. H. Bhatt, Phys. Rev. Lett. **61**, 2817 (1988); see also F. K. McGowan, N. R. Johnson, I. Y. Lee, and C. Baktash, *ibid.* **61**, 2818 (1988).
[11] F. K. McGowan, N. R. Johnson, I. Y. Lee, C. Baktash, J. W. McConnell, M. N. Rao, M. Oshima, J. C. Wells, A. Larabee, L. L. Riedinger, R. Bengtsson, and Z. Xing, Nucl. Phys. **A530**, 490 (1991).
[12] G. Mamane, Ph.D thesis, Weizmann Institute of Science, Rehovot, 1983.
[13] G. Mamane, E. Cheifetz, E. Dafni, A. Zemel, and J. B. Wilhelmy, Nucl. Phys. **A454**, 213 (1986).
[14] A. M. Bergdolt, J. Chevallier, J. C. Merdinger, E. Bozek, and Z. Stachura, in *Proceedings of the International Conference on Nuclear Structure,* Abstracts, Tokyo, 1977, p. 359.
[15] T. Katou, Y. Tendow, H. Kumagi, Y. Gono, and A. Hashizume, in *Proceedings of the International Conference on Nuclear Physics,* Abstracts, Berkeley, 1980, p. 751.
[16] P. F. Mantica, P. K. Joshi, S. J. Robinson, E. F. Zganjar, R. L. Gill, W. B. Walters, D. Rupnik, H. K. Carter, J. Kormicki, and C. R. Bingham, in *Proceedings of the Sixth International Conference on Nuclei Far From Stability*, Bernkastel-Keus, 1992, edited by R. Neugart and A. Wöhr (Inst. of Phys., Bristol, 1993), p. 667.
[17] W. Kutschera, W. Dehnhardt, O. C. Kistner, P. Kump, B. Povh, and H. J. Sann, Phys. Rev. C **5**, 1658 (1972).
[18] A. Chaudhury, M. W. Drigert, E. G. Funk, J. W. Mihelich, and U. Garg, Bull. Am. Phys. Soc. **30**, 742 (1985).
[19] P. von Brentano (private communication quoted in Ref. [1]).
[20] A. Dewald, P. Petkov, R. Wrzal, G. Siems, R. Wirowski, P.

Sala, G. Böhm, A. Gelberg, K. O. Zell, P. von Brentano, P. J. Nolan, A. J. Kirwan, D. J. Bishop, R. Julin, A. Lampinen, and J. Hattula, in *Proceedings of XXV Zakopane School on Physics*, edited by J. Styczén and Z. Stachura (World Scientific, Singapore, 1990), p. 152; see also A. Dewald, Prog. Part. Nucl. Phys. **28**, 409 (1992).

[21] J. C. Walpe, B. F. Davis, S. Naguleswaran, W. Reviol, and U. Garg, Bull. Am. Phys. Soc. **38**, 980 (1993); (private communication).

[22] Ch. Droste, T. Morek, S. G. Rohoziński, D. Alber, H. Grawe, and D. Chelbowska, J. Phys. G **18**, 1763 (1992).

[23] P. Sala, Ph.D thesis, University of Köln, 1993.

[24] P. Petkov, R. Krucken, A. Dewald, P. Sala, G. Böhm, J. Altmann, A. Gelberg, P. von Brentano, R. V. Jolos, and W. Andrejtscheff, Nucl. Phys. **A568**, 572 (1994).

[25] D. M. Gordon, L. S. Eytel, H. deWaard, and D. E. Murnick, Phys. Rev. C **12**, 628 (1975).

[26] E. Hammarén, K. W. Schmid, F. Grümmer, A. Faessler, and B. Fladt, Nucl. Phys. **A454**, 301 (1986).

[27] K. W. Schmid and F. Grümmer, Rep. Prog. Phys. **50**, 731 (1987).

[28] F. Iachello and A. Arima, *The Interacting Boson Model* (Cambridge University Press, Cambridge, England, 1987); F. Iachello and P. Van Isacker, *The Interacting Boson-Fermion Model* (Cambridge University Press, Cambridge, England, 1987).

[29] T. Otsuka, X. W. Pan, and A. Arima, Phys. Lett. B **247**, 191 (1990); see also G. Puddu, O. Scholten, and T. Otsuka, Nucl. Phys. **A348**, 109 (1980).

[30] C. -L. Wu, D. H. Feng, and M. Guidry, in *Advances in Nuclear Physics,* edited by J. W. Negele and E. Vogt (Plenum, New York, 1994), Vol. 21, p. 227.

[31] C. -L. Wu (private communication).

[32] W. Nazarewicz and I. Ragnarsson, in *Nuclear Decay Modes*, edited by D. N. Poenaru and W. Greiner (Oxford University Press, Oxford, in press).

[33] P. Möller and J. R. Nix, Nucl. Phys. **A536**, 20 (1992).

[34] P. Möller and J. R. Nix, Data Nucl. Data Tables **39**, 213 (1988).

[35] V. M. Strutinsky, Yad. Fiz. **3**, 614 (1966) [Sov. J. Nucl. Phys. **3**, 449 (1966)]; Nucl. Phys. **A95**, 420 (1967); **A122**, 1 (1968).

[36] J. J. Lipkin, Ann. Phys. (N.Y.) **9**, 272 (1960); Y. Nogami, Phys. Rev. **134**, B313 (1964); H. C. Pradhan, Y. Nogami, and J. Law, Nucl. Phys. **A201**, 357 (1973).

[37] P. Möller, J. R. Nix, W. D. Myers, and W. J. Swiatecki, At. Data Nucl. Data Tables **59**, 185 (1995).

[38] S. Ćwiok, J. Dudek, W. Nazarewicz, J. Skalski, and T. Werner, Comput. Phys. Commun. **46**, 379 (1987).

[39] J. Dudek, Z. Szymański, and T. R. Werner, Phys. Rev. C **23**, 920 (1981).

[40] T. R. Werner (private communication). In this work, we have chosen to use our own values calculated with the Woods-Saxon model. The differences with Werner's values are minor.

[41] J. D. Walecka, Ann. Phys. (N.Y.) **83**, 491 (1974); B. D. Serot and J. D. Walecka, Adv. Nucl. Phys. **16**, 1 (1986).

[42] Y. K. Gambhir, P. Ring, and A. Thimet, Ann. Phys. (N.Y.) **198**, 132 (1990).

[43] P. Ring and P. Schuck, *The Nuclear Many-Body Problem* (Springer-Verlag, Berlin, 1982).

[44] J. Dobaczewski, I. Hamamoto, W. Nazarewicz, and J. A. Sheikh, Phys. Rev. Lett. **72**, 981 (1994).

[45] C. J. Horowitz and B. D. Serot, Phys. Lett. **137B**, 287 (1984).

[46] P.-G. Reinhard, M. Rufa, J. Maruhn, W. Greiner, and J. Friedrich, Z. Phys. A **323**, 13 (1986); P.-G. Reinhard, Rep. Prog. Phys. **52**, 439 (1989).

[47] H. Toki, Y. Sugahara, D. Hirata, B. V. Carlson, and I. Tanihata, Nucl. Phys. **A524**, 633 (1991).

[48] J. A. Sheikh and P. Ring, Phys. Rev. C **47**, R1850 (1993); J. A. Sheikh, *ibid.* **48**, 476 (1993).

[49] M. M. Sharma, M. A. Nagarajan, and P. Ring, Phys. Lett. B **312**, 377 (1993).

[50] A. Baran, J. L. Egido, B. Nerlo-Pomorska, K. Pomorski, P. Ring, and L. M. Robledo, J. Phys. G **21**, 657 (1995). In addition to RMF results, this paper presents results obtained using mean-field Hamiltonians with Gogny and Skyrme forces. Except for $^{118}Xe_{64}$, the results obtained with Skyrme (Sk7) forces are in good agreement with experiment.

[51] A. K. Dutta, J.-P. Arcoragi, J. M. Pearson, R. Behrman, and F. Tondeur, Nucl. Phys. **A458**, 77 (1986); F. Tondeur, A. K. Dutta, J. M. Pearson, and R. Behrman, *ibid.* **A470**, 93 (1987); J. M. Pearson, Y. Aboussir, A. K. Dutta, R. C. Nayak, M. Farine, and F. Tondeur, *ibid.* **A528**, 1 (1991); Y. Aboussir, J. M. Pearson, A. K. Dutta, and P. Tondeur, *ibid.* **A549**, 155 (1992).

[52] J. M. Pearson and P. Tondeur (private communication).

[53] P. Bonche, H. Flocard, P.-H. Heenen, S. J. Krieger, and M. S. Weiss, Nucl. Phys. **A443**, 39 (1985); P. Quentin and H. Flocard, Annu. Rev. Nucl. Sci. **238**, 523 (1985).

[54] N. Tajima, N. Onishi, and S. Takahara (private communication).

[55] B. Nerlo-Pomorska, K. Pomorski, M. Brack, and E. Werner, Nucl. Phys. **A462**, 252 (1987); B. Nerlo-Pomorska, K. Pomorski, and B. Skorupska-Mach, *ibid.* **A562**, 80 (1993).

[56] B. Nerlo-Pomorska and B. Mach, At. Data Nucl. Data Tables (to be published).

[57] A. Bohr and B. R. Mottelson, *Nuclear Structure* (Benjamin, New York, 1969), Vol. 1, p. 169.

[58] T. Morikawa, M. Oshima, T. Sekine, Y. Hatsukawa, S. Ichikawa, H. Iimura, A. Osa, M. Shibata, and A. Taniguchi, Phys. Rev. C **46**, R6 (1992).